Journal of Molecular Liquids 255 (2018) 313–323

Contents lists available at ScienceDirect

Journal of Molecular Liquids

journal homepage: www.elsevier.com/locate/molliq

The synthesis and application of the SiO_2@Fe_3O_4@MBT nanocomposite as a new magnetic sorbent for the adsorption of arsenate from aqueous solutions: Modeling, optimization, and adsorption studies

Amir Sheikhmohammadi [a], Zohreh Dahaghin [b], Seyed Mohsen Mohseni [c], Maryam Sarkhosh [d,*], Hossein Azarpira [e,*], Zahra Atafar [f], Mehrnoosh Abtahi [g], Shoheila Rezaei [h], Mahdieh Sardar [g], Hassan Masoudi [i], Majid Faraji [j], Shahram Nazari [k], Rokhsane Hosseini Pouya [l], Mohammad Almasian [m]

[a] Students Research Office, Department of Environmental Health Engineering, School of Health, Shahid Beheshti University of Medical Sciences, Tehran, Iran
[b] Young Researchers and Elite Club, Central Tehran Branch, Islamic Azad university, Tehran, Iran
[c] Department of Environmental Health Engineering, School of Health, Qom University of Medical Sciences, Qom, Iran
[d] Social Determinants of Health Research Center, Mashhad University of Medical Sciences, Mashhad, Iran
[e] Department of Environmental Health Engineering, Social Determinants of Health Research Center, Saveh University of Medical Sciences, Saveh, Iran
[f] Department of Environmental Health Engineering, School of Public Health, Tehran University of Medical Sciences, Tehran, Iran
[g] Department of Environmental Health Engineering, School of Health, Shahid Beheshti University of Medical Sciences, Tehran, Iran
[h] Social Determinants of Health Research Center, Yasuj University of Medical Sciences, Yasuj, Iran
[i] Department of chemistry, Payame Noor University, Tehran, Iran
[j] Research Center for Environmental Determinants of Health (RCEDH), Kermanshah University of Medical Sciences, Kermanshah, Iran
[k] Students Research Office, Department of Environmental Health Engineering, School of Health, Ardabil University of Medical Sciences, Ardabil, Iran
[l] Food and Cosmetic Health Research Center, Hormozgan University of Medical Sciences, Bandar Abbas, Iran
[m] Department of the English Language, School of Medicine, Lorestan University of Medical Sciences, Khorramabad, Iran

ARTICLE INFO

Article history:
Received 14 August 2017
Received in revised form 14 January 2018
Accepted 27 January 2018
Available online 31 January 2018

Keywords:
Arsenate
SiO_2@Fe_3O_4@MBT
R software
Modeling
Response surface methodology

ABSTRACT

This study was conducted for the purpose of showing that the mercaptobenzothiazole (MBT)-functionalized SiO_2@Fe_3O_4 nanocomposite can be applied as a new adsorbent for the adsorption of As (V) ions from aqueous solutions. SiO_2@Fe_3O_4@MBT synthesized via a two-stage process was characterized by scanning electron microscopy (SEM), Fourier transform infrared spectroscopy (FTIR), X-ray diffraction (XRD), the transmission electron microscope (TEM) and Brunauer-Emmett-Teller (BET). The SEM showed good adsorbing capacity for SiO_2@ Fe_3O_4@ MBT due to the average core size 40 nm with a vast surface. The appearance of bands attributed to the C—H stretch of methylenes of the alkyl chain in FTIR analysis showed SiO_2@Fe_3O_4 was successfully modified by MBT. The XRD spectrum clearly demonstrates the occurrence of two phases of iron oxide/hydroxide and silica oxide, and also the spinal structure of SiO_2@ Fe_3O_4@ MBT reveals the presence of SiO_2, by revealing the specific peaks at $2\theta = 26.62, 39.44, 42.41, 54.83$.The TEM micrograph of SiO_2@ Fe_3O_4@ MBT showed the Fe_3O_4 nanoparticle anchored on SiO_2 and formed a large amount of Fe_3O_4 with different size. Surface area of SiO_2@ Fe_3O_4@ MBT was investigated and determined 58.35 m^2/g. Response surface methodology (RSM) was employed to model the effects of the operating parameters, such as pH (2–8), adsorbent dosage (10–100 mg L^{-1}), initial As (V) concentration (1–10 mg L^{-1}), and contact time (2–180 min) using the R software. Based on the results obtained from the analysis of variance (ANOVA), the reduced full second-order model demonstrated satisfactory adjustment with the experimental data. The Solver "Add-ins" were applied using the effective parameters to optimize important operating variables. The optimum operating points were established at the initial As (V) concentration of 10 mg L^{-1}, the adsorbent dosage of 82.7 mg L^{-1}, the time of 169.1 min, and the pH of 5.07, corresponding to the maximum predicted As (V) removal percentage of 93.89%. Based on the reported results, the experimental isotherm data best fit the Freundlich model rather than the other isotherms. The maximum adsorption capacities calculated from the Langmuir equation were 10.38, 11.35, and 17.5 mg g^{-1} for 291 K, 301 K and 311 K. The followed kinetic model was the pseudo-first order kinetic model in nature and intraparticle diffusion was the dominant mechanism.

* Corresponding authors.
E-mail addresses: Marya.sarkhosh@yahoo.com (M. Sarkhosh), Hazarpira912@gmail.com (H. Azarpira).

https://doi.org/10.1016/j.molliq.2018.01.164
0167-7322/

1. Introduction

Arsenite (AsO_3^{3-}) and arsenate (AsO_4^{3-}) are the main inorganic forms of arsenic and are highly toxic substances in aqueous solutions [1]. The presence of high concentrations of arsenic (AsO_3^{3-} and AsO_4^{3-}) in ground waters can pose a wide range of risks such as carcinogenic health effects, bladder and lung cancers, nervous and skin pigmentation disorders, such that it has been characterized as a significant concern by many countries [1–3]. Arsenite is more toxic to biological systems than arsenate but under oxidizing conditions, arsenite is unstable and can be oxidized to arsenate. Therefore, the WHO has issued guidelines that recommend that the maximum contamination level of arsenic should be decreased to 10 μg L^{-1} in drinking water [2]. Scientists are studying advantageous technologies that can be used to treat such pollutants [4,5]. Due to simple operation, large surface areas, great adsorption capacity, and also green and easy handling, the use of nano-adsorbents (such as nano-SiO_2) can be an attractive method for the attenuation of pollutants from aqueous solutions [6–9]. The main characteristics of nano-SiO_2 are high stability and non-toxicity [10–13]. Some researchers have reported the emerging application of Fe_3O_4@SiO_2 in the removal of phosphate [14], Cu(II) ions [15], chloroauric ion [11] and methylene blue [16]. Because of having favorable conditions, the surface of nano-SiO_2 can be improved by chelating ligands resulting in very high metal binding capabilities [1]. In recent years, 2-mercaptobenzothiazole (MBT) has been widely used as a chelating ligand in order to form complex compounds with metal ions. Therefore, in the present study, MBT was employed as a suitable surface modification reagent for nano-SiO_2 in the sequestration of arsenate from water solutions [17]. The use of optimization techniques in the application of SiO_2@Fe_3O_4@MBT on an industrial scale can be beneficial, because it improves process efficiency and minimizes operational costs and time. The classical method of changing one factor and fixing the others has some drawbacks, including: 1- It does not take the interactive effects of parameters into consideration. 2- It requires spending a lot of time and performing numerous tests. Therefore, it cannot be as reliable a method as expected [18–21]. To deal with the limitations of the classical method, RSM is applied as a multivariate system and a useful technique, in which all factors are varied simultaneously, resulting in the reduction of the required time and overall operation costs [1]. In some studies, RSM has been implemented by commercial software, such as Design-Expert [22], JMP [23], and Statgraphics [24]. These commercial applications have some restrictions, e.g., they do not generate the various RSM models, which reduce the accuracy of the RSM modeling [25]. The R software with the most standards for first and second order designs and methods for one response variable removes these limitations. This software provides information about how well the model fits the data (lack of fit), estimates all the coefficients in the model, allows blocking of experiments, allows specified variance criteria for estimated coefficients and estimated responses to be met, and also requires as few experiments as possible ([25–27]. In this research, SiO_2@Fe_3O_4 nanocomposites were synthesized and modified with MBT for the first time (that has not yet been reported in detail) based on the idea that this chemical will improve the SiO_2@Fe_3O_4 adsorption capacity for arsenate. The present study was undertaken: (i) to optimize and find an appropriate functional relationship between the response and related input variables by RSM using central composite design (CCD) (ii) to obtain the optimum conditions of the model equation as predicted by RSM using the Solver 'Add-ins' (iii) and to study various isotherm models and kinetic equations to identify the possible adsorption mechanism.

2. Materials and methods

2.1. Chemicals

All chemicals were of reagent grade and doubly distilled water (DDW) was used throughout this work. SiO_2 powder, 2-mercaptobenzothiazole (MBT), H_2SO_4, $FeCl_3.6H_2O$, $FeSO_4.7H_2O$, NH_4OH, and sodium nitrate ($NaNO_3$) were purchased from Sigma-Aldrich, Ltd. Co. The arsenate stock solution was prepared from the sodium arsenate ($Na_2HAsO_4.7H_2O$) (Merck Co). The working solutions of arsenate were obtained by appropriate dilution of the stock solution.

2.2. Synthesis of the SiO_2@Fe_3O_4 magnetic nanocomposite and the MBT-functionalized SiO_2@Fe_3O_4 nanocomposite

The SiO_2@Fe_3O_4 nanocomposite was synthesized using a previously reported procedure [11]. About 0.1 g of SiO_2 was dispersed in 25 mL of deionized water by ultrasonic irradiation for 5 min. Then, a solution of 256.5 mg of $FeCl_3.6H_2O$ and 132 mg of $FeSO_4.7H_2O$ in 25 mL of deionized water were prepared. This mixture was added to the SiO_2 solution and was stirred for 30 min [11,28]. At last, 3 mL of NH_4OH (25%) aqueous solution was added dropwise into the mixture, and then the mixture was kept under constant stirring at 90 °C for 4 h. After 12 h stirring at 40 °C, the Fe_3O_4@SiO_2 was separated by a strong magnet, washed with ethanol and then dried at room temperature [28,29]. The MBT-functionalized SiO_2@Fe_3O_4 nanocomposite was prepared using 2-mercaptobenzothiazole (MBT) based on the method discussed previously [30]. A saturated solution of MBT was prepared and sonicated for 2 h and then the solution was filtered to remove the undissolved MBT by filtration through a 0.45 μm filter membrane. Next, 1.0 g of the Fe_3O_4@SiO_2 nanocomposite was added to the saturated solution of MBT and stirred for 2 days, then the solid Fe_3O_4@SiO_2 nanocomposites were collected using an external magnetic field and washed with deionized water to remove excess MBT, until it became colorless. The final product, the SiO_2@Fe_3O_4@MBT nanocomposite, was dried in an oven at 60 °C overnight. The formation of the SiO_2@Fe_3O_4@MBT nanocomposite was confirmed by IR spectroscopy and scanning electron microscopy [28,29,31,32]. The schematic of the SiO_2@Fe_3O_4@ MBT nanocomposite is portrayed in Fig. 1.

2.3. Sorbent characterization and analytical methods

The surface structure and elemental analysis of the prepared adsorbent was done by SEM (JEOL-JED 2300AnalysisStatio). The FT-IR spectra of the products were recorded on the Fourier-Transform Infrared (FT-IR, Shimadzu Prestige21) with KBr pellets (Bruke EQUINOX 55 Germany). The infrared spectra were measured within the range of 40–4000 cm^{-1}. The XRD data were acquired on an X-ray diffractometer (Shimadzu S-6000) with Cu K_a irradiation ($\lambda = 1.5406$ Å). A transmission electron microscope (TEM) at 180 kV was used to analyze the surface morphology.

2.4. Factorial experimental design and the optimization of the parameters

Response surface methodology comprises a body of methods for exploring the optimum operating conditions through experimental methods. Typically, this involves several steps: (1) coding of data (2) generating a design (3) fitting a response surface model (4) displaying a response surface (5) optimization [33]. The R software for windows (version 3.0.3:6 March 2014) was used for this purpose [34,35]. In the R software, the CCD function is available to generate the standard response surface design consisting of 2^k points that form the base design, 2k star points (axial points), and several center points where k is the number of variables [30]. The CCD levels designed for 4-input independent factors included pH (X_1), SiO_2@ Fe_3O_4@ MBT dosage (X_2), time (X_3) and initial As (V) concentration (X_4), which are given in Table 1. Generally, 28 runs were designed using 16 factorial points and 12 center points. Next, the output-dependent response variable (removal efficiency (Υ)) related to each run was determined via experimental methods. The R software embraces three models of RSM: (i) the first-order response-surface model (FO), (ii) the two-way interactions model (TWI) and (iii) the full second-order model (FSO)

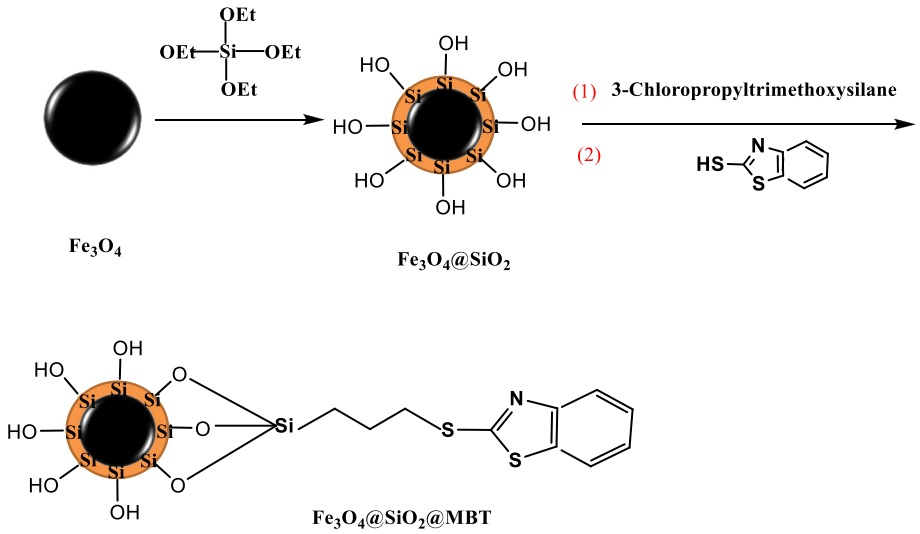

Fig. 1. The schematic representation of the synthesis of Fe_3O_4, the magnetic SiO_2 -Fe_3O_4 nanocomposite and the MBT-functionalized SiO_2 -Fe_3O_4 nanocomposite.

[35]. To obtain a suitable response surface model, data was fitted with the three models of RSM and the best model was selected for the optimization process and further analysis. Additionally, the reduced model was applied if it was required. Four parameters, including F-value, p-value, multiple R-squared (R^2) and lack of fit, were taken into account in the evaluation of the models. The criteria for the selection of the appropriate model included greater F-value, smaller p-value, higher R^2 and insignificant lack of fit (or more lack of fit). The adequacy of the fitting of the models was further justified by ANOVA analysis [21]. Eq. (1) was used to estimate the relationship between the independent and the experimental responses:

$$\Upsilon = b_0 + \sum_{i=1}^{k} b_i X_i + \sum_{i=1}^{k} b_{ii} X_i^2 + \sum_{i=1}^{k-1} \sum_{j=1}^{k} b_{ij} X_i X_j + C \quad (1)$$

where b_0 is the intercept value, bi, bii, and bij refer to the regression coefficient for the linear, second order, and interactive effects, respectively, Xi and Xj are the independent variables, and C denotes the error of prediction [25,36]. Finally, to obtain the optimum conditions, the Solver 'Add-ins' were applied using effective parameters to write the model equation as predicted by RSM [25,37].

2.5. Batch experiments

Sodium (meta) arsenate (Sigma-Aldrich, 99%) was used in order to prepare the arsenate stock solution (1 mg As cm^{-3}), and the desired As (V) concentrations were obtained by the dilution of the stock solution. All the experiments were carried out according to the runs determined by the RSM method inside 250 mL Erlenmeyer flasks containing 100 mL of arsenate solution. The mixtures were shaken at 200 rpm for a predetermined time period. Then, samples were withdrawn from the solution and centrifuged at 3000 rpm. After filtering the samples through 0.22 μm syringe filters, the residual concentration of arsenate was analyzed using a graphite furnace atomic absorption spectrometer.

Table 1
The actual and coded values of the independent variables used for the experimental design.

Variable	Symbol	Coded level		
		−1	0	1
			Real values	
pH	X_1	2	5	8
SiO_2@ Fe_3O_4@ MBTdose (g L^{-1})	X_2	10	55	100
Time (min)	X_3	2	91	180
As (V) concentration (mg L^{-1})	X_4	1	5.5	10

2.6. Isotherm study

Equilibrium experiments were conducted under the optimum conditions obtained from the model at various temperatures (291, 301 and 311 K) for initial As (V) concentrations of 1 to 10 mg L^{-1}. To obtain maximum sorption, the mixture was shaken for 3 h at 180 rpm. The adsorption results were then analyzed using the Langmuir, Freundlich, Temkin and Dubinin–Radushkevich (D–R) isotherm models in order to determine the relationship between equilibrium capacity and equilibrium concentration. The linear shape of the Langmuir model (based on the assumption of a homogenous surface energy distribution) is presented in Eq. (2) [38,39]:

$$\frac{c_e}{q_e} = \frac{1}{q_m b} + \frac{1}{q_m} c_e \quad (2)$$

where q_e, C_e, q_m and b are the equilibrium amounts of the adsorbate (mg g^{-1}), the equilibrium concentration of the adsorbate (mg L^{-1}), the maximum adsorption capacity (mg g^{-1}), and the Langmuir constant related to the binding site (L mg^{-1}), respectively. The Langmuir isotherm model is described based on the R_L parameter (Eq. (3)), which is unfavorable for $R_L > 1$, linear for $R_L = 1$, favorable for. $0 < R_L < 1$ and irreversible for $R_L = 0$. C_0 is the highest initial concentration of As (V) ion (mg L^{-1}).

$$R_L = \frac{1}{[1 + bc_0]} \quad (3)$$

The linear shape of the Freundlich isotherm model (appropriate for heterogeneous systems) is expressed by Eq. (4) [40]:

$$\log q_e = \log k_f + \frac{1}{n} \log c_e \quad (4)$$

where K_f ($mg^{1-1/n}/L^{1/n}/g$) and 1/n are the Freundlich constants, related to the adsorption capacity and intensity, respectively. The value of "n" denotes the adsorption process and the value of 1/n should be in the range of 0.1–1 for a favorable adsorption.

The Temkin isotherm is also available for heterogeneous surface adsorption. The linear form of the Temkin model is given by Eq. (5) [38]:

$$q_e = B_1 \ln(k_t) + B_1 \ln(C_e) \quad (5)$$

where $B_1 = RT/b_1$ (R is the universal gas constant and T is the absolute temperature), b_1 and k_t are the adsorption heat (kJ mol^{-1}) and the equilibrium binding constant (L g^{-1}) corresponding to the maximum binding energy, respectively. A high value of b_1 and a low k_t value depict a fast sorption of the adsorbate at the initial stage and weak bonding of the adsorbate onto the medium, respectively.

Also arsenate adsorption data have been analyzed by Dubinin–Radushkevich isotherm model. The linear form of the D-R is given by Eq. (6).

$$\ln qe = \ln q_m - K_{DR}\varepsilon^2 \quad (6)$$

where K_{DR} is a constant related to mean free energy of sorption per mol of the sorbate [mg^2 kJ^{-2}] and ε is Polanyi potential [J mg^{-1}]. K_{DR} can be calculated from the slope of the linear plot of ln q_e versus ε^2. Also ε can be obtained using following equation:

$$\varepsilon = RT\ln(1 + 1/C_e) \quad (7)$$

where R is the universal gas constant [8.314 kJ/kmol·K] and T[K] is the absolute temperature. The mean free energy of adsorption [E] can be written as:

$$E = 1/[2K_{DR}]^{0.5} \quad (8)$$

If the value of E be between 8 and 16 kJ mol^{-1}, the adsorption process is chemical and if be less than 8 kJ mol^{-1}, the adsorption process is physical.

2.7. Kinetic study

An adsorption kinetic study was conducted using equilibrium time data. For this purpose, under optimum conditions obtained from the RSM model, 100 mL As (V) solution (1, 2 and 3 mg L^{-1}) was placed inside 250 mL Erlenmeyer flasks, and samples were taken at regular time intervals (2–180 min). The three kinetic models, including the pseudo-first order, pseudo-second order, and intra-particle diffusion models, were considered. The pseudo-first order kinetic (the linear equation) is described by the following Eq. (9) [25,41]:

$$\log q_e - q_t = \log q_e - \frac{k_1}{2.303}t \quad (9)$$

where q_e, q_t are the amounts (mg g^{-1}) of the adsorbate at equilibrium and at time t (min), respectively. k_1 (min^{-1}) is the rate constant of the pseudo-first order model. The pseudo-second order kinetic is expressed by Eq. (10):

$$\frac{t}{q_t} = \frac{1}{k_2 q_e^2} + \frac{1}{q_e}t \quad (10)$$

where k_2 (g mg^{-1} min^{-1}) is the rate constant of the pseudo-second order model.

In order to gain insight into the mechanisms and rate controlling steps affecting the kinetics, the data were tested using the intra-particle diffusion model that is given as follows in Eq. (11):

$$q_t = k_d t^{1/2} + I \quad (11)$$

where k_d is the intra-particle diffusion rate constant (mg g^{-1} min$^{-1/2}$) and I is a constant that gives an idea about the thickness of the boundary layer [38,42].

2.8. The determination of the zero point charge

In order to investigate to what extent the surface charge of the adsorbent material depended on pH, the zero point charge (pH_{zpc}) was determined by adding 50 mL of the potassium nitrate (0.01 M) solution to Erlenmeyer flasks containing 0.2 g of the adsorbent. The solution pH was set to the desirable values in the range of 2 to 12 by adding HCl and NaOH. The mixture was shaken for 24 h. The final pH of each beaker was measured using a pH meter (Model Sartorius PP-50). The intersection point of the initial pH versus the final pH was recorded as pH_{zpc} (7.87) [38].

3. 3. Results and discussion

3.1. Characterization results

The morphological and surface structural characteristics of the SiO_2@Fe_3O_4@MBT nanocomposite were investigated using SEM (Hitachi- S4160, Tokyo, Japan). The SEM pattern in Fig. 2a showed that the average SiO_2@ Fe_3O_4@ MBT core size was approximately 40 nm with a vast surface that is indeed responsible for its good adsorbing capacity. To further investigation of the surface morphology, the TEM micrograph of SiO_2@ Fe_3O_4@ MBT was recorded (Fig. 2b). Fig. 2b portrayed the Fe_3O_4 nanoparticle anchored on SiO_2 and formed a large amount of Fe_3O_4 with different size. The structure of the SiO_2@ Fe_3O_4@MBT sample was characterized using FTIR spectroscopy. The FT-IR was employed to examine the surface groups of the synthesized materials, and their spectra are portrayed in Fig. 3. The IR spectrum of SiO_2@Fe_3O_4 was characterized as follows (cm^{-1}): 580 (Fe—O), 3400 (O—H), and 3394 (COOH). There also appeared a broad strong band

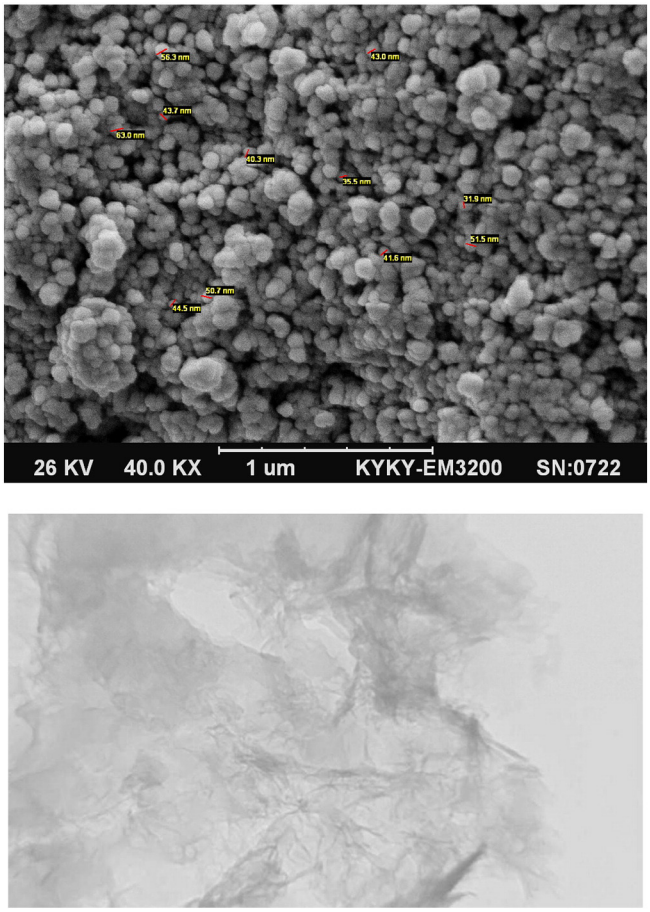

Fig. 2. SEM (a) and TEM (b) images of the MBT-functionalized SiO_2-Fe_3O_4 nanocomposite.

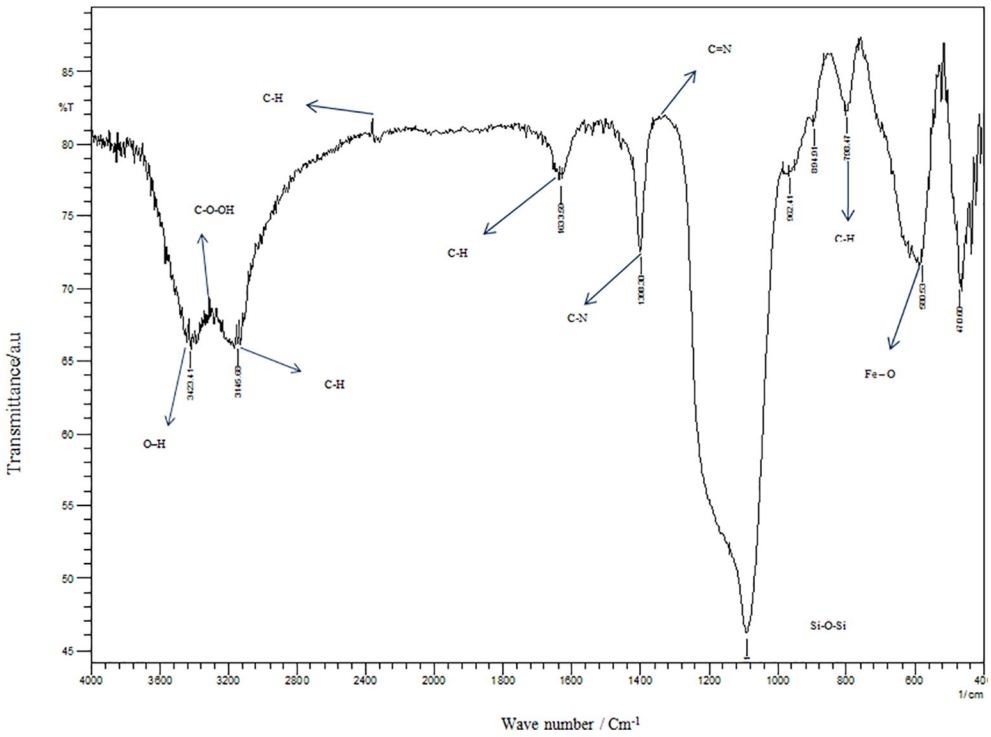

Fig. 3. The FTIR spectra for the SiO_2@ Fe_3O_4@ MBT nanocomposite.

at around 1100 cm^{-1} due to Si-O-Si stretching. Furthermore, the presence of signals at 1575 cm^{-1} (C═N) and 1107 cm^{-1} (C—N) proved. The appearance of bands at 2900 and 2850 cm^{-1} was attributed to the C—H stretch of methylenes of the alkyl chain which showed SiO_2@Fe_3O_4 was successfully modified by MBT (The functional groups related to the surface functionalization with 2-mercaptobenzothiazole are peaks for substituted benzene, carbonyl groups and the CH of alkenes at 796, 1625 and 2952 cm^{-1}). Fig. 4 shows the X-ray diffraction (XRD) pattern of the SiO_2@Fe_3O_4@MBT nanocomposite. The XRD spectrum clearly demonstrates the occurrence of two phases of iron oxide/hydroxide and silica oxide. There are peaks located at 30.1°, 35.4°, 43.1°, 53.4°, 56.9°, and 62.5°, which are indexed to (220), (311), (400), (422), (511), and (440), respectively. They can be related to lattice planes. The spinal structure of SiO_2@ Fe_3O_4@ MBT reveals the presence of SiO_2, by revealing the specific peaks at 2θ = 26.62, 39.44, 42.41, 54.83.

In the BET analysis, surface area of SiO_2@ Fe_3O_4@ MBT was investigated and determined 58.35 m^2/g. The pore size distribution curve showed average pore diameter and average particle size of 10.18415 nm and 102.8184 nm respectively.

3.2. The magnetism strength of the SiO_2@ Fe_3O_4@ MBT

In order to determine sufficient magnetization of SiO_2@Fe_3O_4@MBT for separation in water treatment, the magnetic field strength of SiO_2@ Fe_3O_4@MBT analyzed. As portrayed in Fig. 5, with an increasing in field from −2 to 8 Tesla (One tesla is equal to one weber per square meter), a sharp increase in magnetization was observed as the magnetization at about 7 Tesla reached to saturation mod. As shown in Fig. 5 from −1.5 to 1.5 Tesla a ferromagnetic hysteresis state was created. The saturation magnetization of SiO_2@Fe_3O_4@MBT was 7.194 Tesla; thus, separation of

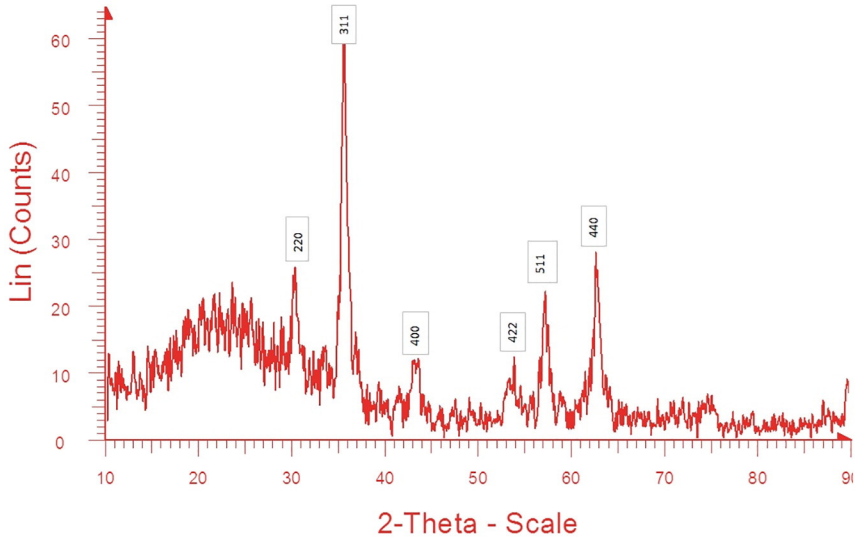

Fig. 4. The XRD pattern for the SiO_2@ Fe_3O_4@ MBT nanocomposite.

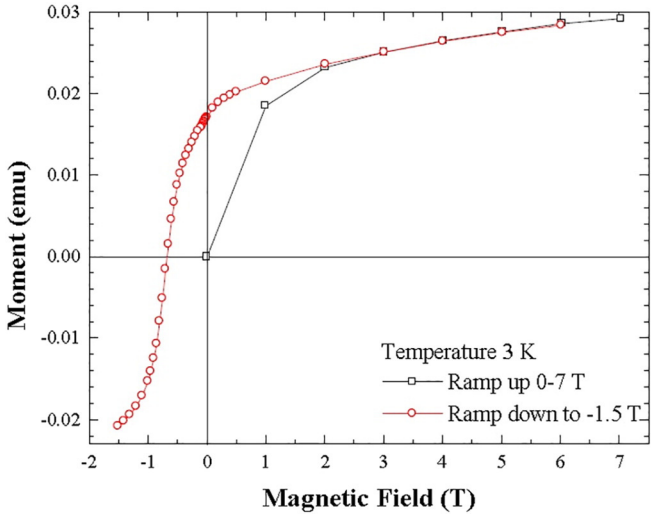

Fig. 5. The magnetism strength of the SiO_2@ Fe_3O_4@ MBT.

Table 2
The central composite design matrix with coded and uncoded values of the independent variables and the experimental and predicted values of the response.

Sl.no.	Coded values				Uncoded values				% Removal	
	X_1	X_2	X_3	X_4	X_1	X_2	X_3	X_4	Expt. (%)	Pred. (%)
1	1	1	1	−1	8	100	180	1	90.60	91.52
2	1	−1	1	−1	8	10	180	1	75.15	74.15
3	0	0	0	0	5	55	91	5.5	68.40	68.93
4	−1	−1	−1	−1	2	10	2	1	34.1	29.97
5	0	0	0	0	5	55	91	5.5	67.1	68.93
6	0	0	0	0	5	55	91	5.5	66.9	68.93
7	0	0	0	0	5	55	91	5.5	66.47	68.93
8	−1	−1	−1	1	2	10	2	10	12.2	12.6
9	−1	1	−1	1	2	100	2	10	32.4	32.14
10	0	0	0	0	5	55	91	5.5	66.00	68.93
11	0	0	0	0	5	55	91	5.5	65.8	68.93
12	−1	1	1	1	2	100	180	10	53.51	66.32
13	0	0	0	0	5	55	91	5.5	65.8	68.93
14	1	−1	−1	1	8	10	2	10	21.4	18.35
15	0	0	0	0	5	55	91	5.5	65.4	68.93
16	0	0	0	0	5	55	91	5.5	63.64	68.93
17	−1	1	1	−1	2	100	180	1	70.1	68.17
18	0	0	0	0	5	55	91	5.5	62.90	68.93
19	0	0	0	0	5	55	91	5.5	62.70	68.93
20	0	0	0	0	5	55	91	5.5	60.5	68.93
21	−1	−1	1	1	2	10	180	10	31.74	46.79
22	1	1	−1	−1	8	100	2	1	55.30	53.07
23	1	1	−1	1	8	100	2	10	42.22	43.82
24	−1	1	−1	−1	2	100	2	1	38.1	41.4
25	1	1	1	1	8	100	180	10	75.9	88.68
26	−1	−1	1	−1	2	10	180	1	52.4	57.73
27	1	−1	−1	−1	8	10	2	1	33.45	35.70
28	1	−1	1	1	8	10	180	10	45.4	63.21

adsorbent from waterby was easily done by an external magnetic field. The remanence was low enough that SiO_2@Fe_3O_4@MBT could be easily re-dispersed for reuse after separating from aqueous solution.

3.3. Fitting a response-surface model and the development of regression model equation

The levels obtained from the R software based on the CCD design, including the independent and dependent variables, are presented in Table 2. Three special models (FO, TWI and FSO) were applied to fit the data. Each model introduced particular information about multiple R-squared, adjusted R-squared, F-statistic, p-value and lack of fit that were too important to specify the response surface portion of the model [25]. The analysis of variance (ANOVA) was applied to delineate the worthiness of the models. The model with an insignificant lack of fit (p-value ˃ 0.05), greater F-value, smaller p-value, and higher R^2 was selected as the most appropriate model. The results obtained for the three models are presented in Table 3. As shown in Table 3, the FO and TWI models showed a breakdown of lack of fit, as the lack of fit value for these models was significant (p-value ˂ 0.05), whereas the FSO model showed an insignificant lack-of-fit (0.081). Moreover, the FSO model presented a greater F-value (150.6), a smaller p-value (8.9×10^{-13}), and a higher R^2 (multiple R-squared: 0.986, adjusted R-squared: 0.977) than the two previous models as is apparent in Table 4. The proximity of the multiple R-squared value to the adjusted R-squared value and R^2_{adj} (0.977) with R^2_{pred} (0.923) (Fig. 6) represents a good chance for significant terms to be included in the model. Therefore, it demonstrated the satisfactory agreement between the FSO model and the experimental data and, therefore, this model can be used for prediction and optimization. The regression analysis of the FSO model (Table 5) indicated that the terms of X_1, X_2, X_3, X_4, X_1: X_2, X_1: X_3, X_2: X_4, X_3: X_4 and X_1^**2** have significant effects (p-values < 0.05) on the removal performance. The terms of X_4, X_1: X_3, X_3: X_4 and X_1^**2** represented an oppositional effect on the model, while other terms indicated an intensifying effect on the response prediction of the model. The obtained equations from the quadratic model, for both coded and actual factors of the parameters are presented below:

A. The final equation in terms of the coded factors:

$$\Upsilon = 65.13 + 7.17\,X_1 + 9.52\,X_2 + 14.09\,X_3 - 8.4\,X_4 - 17.39\,{X_1}^2 + 1.56\,X_1X_2 - 2.73\,X_1X_3 + 2.14\,X_2X_4 - 1.80\,X_3X_4 \quad (12)$$

B. The final equation in terms of the uncoded factors:

$$\Upsilon = -2.14 + 20.14\,X_1 + 0.095\,X_2 + 0.132\,X_3 - 2.036\,X_4 - 1.932\,{X_1}^2 + 0.011\,X_1X_2 + 0.01\,X_1X_3 + 0.01\,X_2X_4 - 0.004\,X_3X_4 \quad (13)$$

3.4. Process optimization and confirmation

The stationary points in original units are very important in achieving the optimum conditions of the model as predicted by RSM, because they estimate some confirmatory data near the optimum conditions and are clear evidence of a nearby set of optimal conditions. The analysis of the FSO model revealed the stationary points are 5.7, 90 mg L^{-1},

Table 3
The comparison of different RSM models for fitting a response-surface model.

Model	Multiple R-squared	Adjusted R-squared	F-statistic	p-value	Lack of fit
First-order response-surface model	0.724	0.676	15.12 on 4 and 23 DF	3.406e−06	2.561e−07
Two-way interactions model	0.758	0.616	5.331 on 10 and 17 DF	0.0013	3.917e−08
Second-order model	0.986	0.977	105.6 on 11 and 16 DF	8.9e−13	0.081

Table 4
The analysis of variance (ANOVA) of the FSO model.

Model formula in RSM	DF	Sum of squares	Mean square	F-value	Probability (P)
First-order response (x_1, x_2, x_3, x_4)	4	6583.3	1645.83	213.3157	1.166e-13
Two-way interaction response (x_3, x_4)	6	306.9	51.15	6.6295	0.001147
Pure quadratic response (x_1, x_2, x_3)	1	2073.6	2073.63	268.7639	2.001e-11
Residuals	16	123.4	7.72	–	–
Lack of fit	5	67.7	13.54	2.6702	0.081118
Pure error	11	55.8	5.07	–	–

Notes: Multiple R-squared: 0.986, Adjusted R-squared: 0.977, PredictedR^2 = 0.923, F-statistic: 105.6 on 11 and 16 DF, p-value: 1.711e−9.

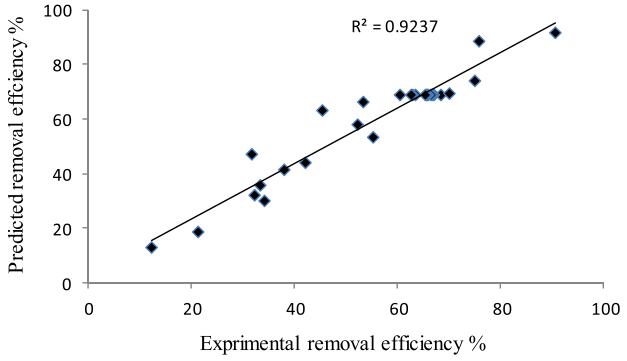

Fig. 6. Experimental arsenate removal efficiency vs. predicted removal efficiency.

172.2 min and 10 mg L^{-1} for X_1, X_2, X_3 and X_4, respectively; therefore, confirmatory data should probably be collected about these results. The Solver 'Add-ins' were applied to obtain the optimum conditions of the model as predicted by RSM. For this purpose, the Solver method is designated with involving parameter values about the stationary point data and entering uncoded regression coefficients. By involving all parameters simultaneously, the maximum removal efficiency was estimated as 93.89%. The optimum conditions of the FSO model (estimated by the Solver 'Add-ins'), were 5.07, 82.7 mg L^{-1}, 169.1 min and 10 mg L^{-1} for pH, SiO_2@Fe_3O_4@MBT dosage, time, and initial As (V) concentration, respectively. Next, an additional experiment was carried out (involving optimum conditions recommended by the Solver 'Add-ins') in order to confirm the validity of the predicted optimum conditions. It was found that the experimental findings (92.37%) were in good agreement with the model prediction (93.89%).

3.5. Response surface methodology and contour plotting

The contour plots based on the presented model coefficients were applied to express the interactive effect of different parameters on the adsorption efficiency and the results are presented in Fig. 7(a, b). Fig. 7 shows the interactive effects of pH (2–8) and time (2–150 min) on the performance of SiO_2@ Fe_3O_4@MBT for the adsorption of arsenate. The pH has a key role on the effectiveness of As (V) adsorption onto SiO_2@ Fe_3O_4@ MBT, because it can affect solubility and the degree of ionization of As (V). As is portrayed in Fig. 7(a), the percentage of arsenate removal was promoted by varying pH from 2 to 6 and was decreased along with the increase of pH after exceeding pH_{pzc} of the adsorbent (pH_{pzc} = 7.87). This is in accordance with the study conducted by Ocin'ski et al. [43]. In other words, at alkaline pH, arsenate occurs in the form of dissociated $H_2AsO_4^-$ and $HAsO_4^{-2}$, which are negatively charged molecules (pK_{a1} = 2.2); therefore, the surface charge of the sorbent has key importance. The surface charge of SiO_2@ Fe_3O_4@ MBT is negative at pH > 7.87 which suppresses the adsorption of anions ($H_2AsO_4^-$ and $HAsO_4^{-2}$), causing a drop in adsorption efficiency [44,45]. The process of As (V) adsorption is independent of ionic strength and dependent on pH value, this leads to the proceeding of the sorption process by the formation of inner-sphere surface complexes on the surface of the sorbent [25]. As shown in Fig. 7(a), the reaction time had no effect on the performance of adsorption and the influence of time was significant at the pH range of 6.0 to 7.0. This phenomenon reveals the interactive effect of the pH and reaction time on the performance of SiO_2@Fe_3O_4@MBT for the adsorption of arsenate, as a certain pH (6.0) and a fixed dosage of the adsorbent (55 g L^{-1}) and an increasing time of 2 to 150 min led to the improvement of adsorption efficiency from 70% to 85%. This can be attributed to more vacant surface sites available for adsorption and the diffusion of arsenate into the bulk of the adsorbent (interior surface). After a certain reaction time, the adsorbent reaches an equilibrium state, which can be due to repulsive forces between the absorbent and absorbate in the aqueous solution that makes the remaining available surface sites difficult to occupy [46,47]. These results are supported by Bandpei et al. [36] and Sheikhmohammadi et al. [25]. The interactive effect of the adsorbent dose (20–100 mg L^{-1}) and initial As (V) concentration (2–10 mg L^{-1}) on the adsorption performance of arsenate by SiO_2@Fe_3O_4@MBT is presented in Fig. 6(b). The adsorbent dosage has a direct relation to the uptake capacity of an adsorbent, which must be carefully adjusted during wastewater treatment. As shown in Fig. 6(b), at a fixed initial As (V) concentration (2 mg L^{-1}), pH (5.0), and reaction time (91 min), with an increase of the adsorbent dose from 20 mg L^{-1} to 100 mg L^{-1}, the adsorption effectiveness increased from 74% to 86%. This can be attributed to the increased active sites/As (V) ratio as the adsorbent dose increases and also the high capacity of the SiO_2@Fe_3O_4@ MBT for the pore diffusion of the As (V) into the bulk of the adsorbent

Table 5
The regression analysis of the reduced quadratic model with coded and uncoded values of the independent variables.

Model term	Coded values				Uncoded values			
	Coefficient estimate	Std. error	t-Value	p-Value	Coefficient estimate	Std. error	t-Value	p-Value
(Intercept)	65.13417	0.80184	81.2305	<2.2e−16	−2.143902	3.878323	−0.553	0.58721
X_1	7.17688	0.69442	10.3351	1.733e−08	20.146791	1.290095	15.617	6.56e−12
X_2	9.52063	0.69442	13.7102	2.919e−10	0.095569	0.036379	2.627	0.01710
X_3	14.09812	0.69442	20.3021	7.593e−13	0.132101	0.018394	7.182	1.10e−06
X_4	−8.39937	0.69442	−12.0956	1.834e-09	−2.036758	0.298080	−6.833	2.14e−06
X_1: X_2	1.56313	0.69442	2.2510	0.038799	0.011579	0.121014	2.192	0.04174
X_1: X_3	−2.73063	0.69442	3.9323	0.001190	0.010227	0.005281	3.830	0.00123
X_2: X_4	2.13938	0.69442	3.0808	0.007162	0.010565	0.002670	3.001	0.00768
X_3: X_4	−1.80813	0.69442	−2.6038	0.019192	−0.004515	0.003521	−2.536	0.02070
X_1^2	−17.38979	1.06074	−16.3940	2.001e−11	−1.932199	0.121014	−15.967	4.51e−12

(interior surface) which can result in an increased tendency of the surface to absorb arsenate ions. However, it is notable that further increments in the sorbent dose may lead to the aggregation of available binding sites resulting in a drop in adsorbent performance in the adsorption of arsenate [36,46]. As portrayed in Fig. 7(b), it can be observed that the removal efficiency of SiO_2@Fe_3O_4@MBT decreases from 74% to 64% as the initial As (V) concentration increases from 2 to 10 mg L^{-1} (at a fixed adsorbent dosage, 20 g L^{-1}, pH 5.0, and reaction time 91 min). This drop in the removal performance can be because of the fixation of the surface binding sites on the adsorbent and the saturation of the binding sites [47].

3.6. Adsorption isotherms

An important step in determining the adsorption capacity of the adsorbent and in investigating the mechanisms of adsorption is the liquid/solid phase metal ion distribution that can be expressed by the equilibrium adsorption isotherms [25,48]. In order to evaluate the experimental results and the adsorption performance, equilibrium data were fitted onto the Langmuir, Freundlich and Temkin isotherm models by an accurate fit of equilibrium data (confirmed by the closeness of regression values). Table 6 indicates the isotherm parameters for the SiO_2@Fe_3O_4@MBT adsorbent showing an accurate fit of the equilibrium data

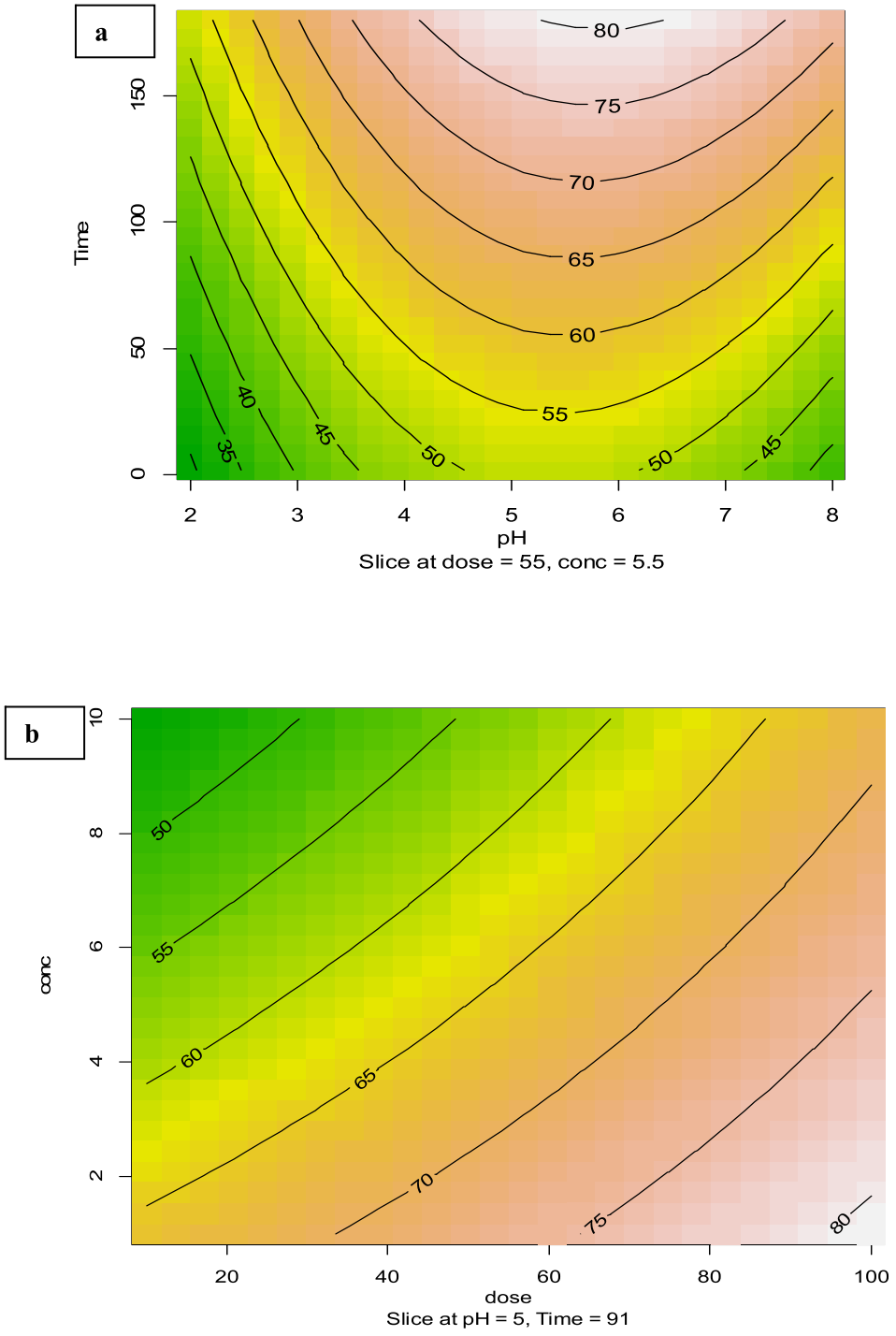

Fig. 7. The contour plot of the combined effects of pH, time (a), the initial concentration of As (V), and the adsorbent dosage (b) on arsenate removal efficiency.

Table 6
The adsorption isotherm parameters for the adsorption of As (V) on SiO_2@Fe_3O_4@MBT at different temperatures.

Isotherm model	T			
		291 K	301 K	311 K
Langmuir	q_m (mg g^{-1})	10.38	11.35	17.5
	b (L mg^{-1})	0.6	1.09	0.7
	R_L	0.14	0.18	0.12
	r^2	0.85	0.91	0.97
Freundlich	K_f ($mg^{1-1/n}/L^{1/n}$/g)	3.5	3.77	3.88
	N	1.61	1.58	1.57
	r^2	0.993	0.997	0.998
Temkin	k_t (L g^{-1})	0.014	0.007	0.005
	b_1	4.76	4.45	4.47
	r^2	0.88	0.92	0.94
D-R	qm (mg g^{-1})	4.8	5.85	6.2
	K_{DR} (mg^2 kJ^{-1})	6×10^{-8}	5×10^{-8}	4×10^{-8}
	E (kJ mg^{-1})	3.33	3.16	3.57
	r^2	0.84	0.93	0.95

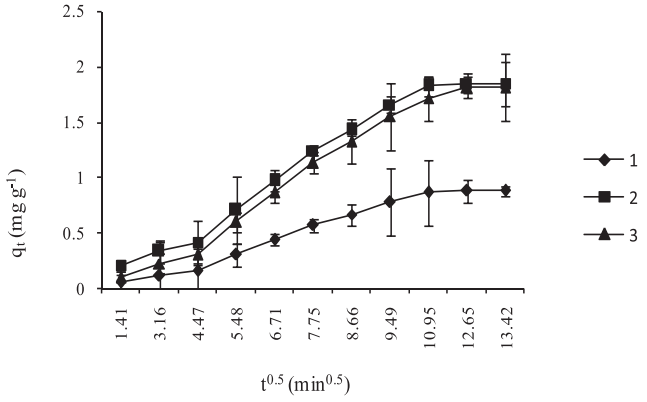

Fig. 8. Intraparticle diffusion model for the adsorption of As (V) onto SiO_2@ Fe_3O_4@MBT

for the three isotherm models. As can be seen from Table 6, there is a slightly higher correlation coefficient for the Freundlich model than that of the rest of the isotherms. This means that the As (V) adsorption onto SiO_2@Fe_3O_4@MBT could be attributed to the multi-molecular layer adsorption, the heterogeneous system, and the uneven adsorption of the adsorbate on the adsorbent surface [49]. Based on the Langmuir model, the maximum capacity (q_m) of SiO_2@ Fe_3O_4@MBT for the As (V) adsorption at the expense of minimum energy (0.6 till 1.09 L mg^{-1}) increased as a result of an increase in temperature and reached from 10.37 to 17.5 mg g^{-1}. Suresh Kumar et al. indicated excellent adsorption capacity at As (V) (47.8 mg g^{-1}) for the iron aluminum hydroxide coated by ontomacroporous supports. The Ma study group announced the maximum adsorption capacity of arsenate by zirconium nanoparticle sorbent to be 256.4 mg g^{-1} [50]. In a study conducted by Velickovic et al., the maximum adsorption capacities obtained from the Langmuir model for As(V) on e-MWCNT/Fe^{2+} and e-MWCNT/Fe^{3+} were 23.47 and 13.74 mg g^{-1} at 25 °C, respectively [51]. The slow sorption of As (V) at the initial stage and the very weak bonding of As (V) on the natural medium surface can be attributed to the low value of the adsorption heat (b_1) and the equilibrium binding constant (k_t), respectively. This revealed the favorable adsorption of As (V) onto SiO_2@ Fe_3O_4@MBT ($n = 1.57$ to 1.61) which was also confirmed by the value of the equilibrium parameter R_L (0.12 to 0.18) [52]. Also the D-R isotherm studied in order to investigate adsorption mechanism type. As D-R isotherm, if the value of E be between 8 and 16 kJ mol^{-1}, the adsorption process is chemical and if be <8 kJ mol^{-1}, the adsorption process is physical. As tabulated in Table 6, for the adsorption of arsenate on to SiO_2@Fe_3O_4@ MBT, the value of E was 3.33, 3.16 and 3.57 kJ mol^{-1} in temperatures of 15, 25 and 35 °C respectively, at which indicates the mechanism of arsenate adsorption on to SiO_2@Fe_3O_4@MBT, is physical.

3.7. Kinetic study

The sorption kinetic study in wastewater treatment is very important, because it provides valuable insights into the reaction pathways and determines mechanism of sorption reaction [14,15]. The parameters of the kinetic models are tabulated in Table 7. The predicted high R^2 values and the agreement of the experimentally observed q_e (q_e, exp) values with the predicted q_e values (q_e, cal) were indicators for the selection of the best model. As shown in Table 7, it can be observed that there are high R^2 values and a good agreement between (q_e, exp) and (q_e, cal) for the pseudo-first order kinetic model in comparison with the pseudo-second order kinetic model. This agreement is indicative of the applicability of the pseudo-first order model to fit the experimental kinetic data for the present system. This reveals As (V) ions are sorbed onto one sorption site on the adsorbent surface and the adsorption was done based on the sorption capacity of solids. The low equilibrium capacity (q_e, cal) and the high rate constant (k_1) (presented in Table 7) depict the shorter time needed to reach equilibrium for the lower concentrations [11,16]. To investigate the adsorption rate controlling step, the data were tested using the intra-particle diffusion model, which gives insight into the mechanisms and rate controlling steps affecting the kinetics. Based on this model, if the plot of q_t versus $t^{0.5}$ is a straight line, intra-particle diffusion is involved in the adsorption process, whereas if multi-linear plots involve various steps, then two or more steps influence the adsorption process. Fig. 8 indicates the intra-particle diffusion plots for the different concentrations of As (V) adsorption onto SiO_2@Fe_3O_4@MBT. It can be observed from Fig. 8 that the plot of q_t versus $t^{0.5}$ is multi-linear for all concentrations, indicating that more than one process is responsible for the adsorption. The initial portion of the plots (first stage) is attributed to instantaneous adsorption or external surface adsorption. This portion is followed by a sharper portion (second stage) where intra-particle or pore diffusion is rate limiting. The plateau portion of the curve (third stage) refers to a slow-down due to intraparticle diffusion because of extremely low adsorbate concentrations left in the solutions (the final equilibrium stage). The comparison of the intraparticle diffusion rate constant (K_d) (calculated from the slope of the second linear section) with K_d parameter given from the first linear section (Table 7) confirms intra-particle diffusion as the dominant mechanism for As (V) adsorption onto SiO_2@ Fe_3O_4@MBT (higher values of K_d for intra-particle diffusion than surface

Table 7
The kinetic parameters for As (V) adsorption onto SiO_2@Fe_3O_4@MBT at different initial concentrations.

C_0 mg L^{-1}	Pseudo-first- order				Pseudo- second- order				Intra- particle diffusion					
									First line (surface diffusion)			Second line (intraparticle diffusion)		
	q_e, exp. (mg g^{-1})	q_e, cal. (mg g^{-1})	k_1 (min^{-1})	R^2	q_e, cal. (mg g^{-1})	k_2 (g mg^{-1} min^{-1})	h_0 (mg g^{-1} min^{-1})	R^2	k_d (mg g^{-1} $min^{-1/2}$)	I (mg g^{-1})	R^2	k_d (mg g^{-1} $min^{-1/2}$)	I (mg g^{-1})	R^2
1	0.87	1.35	0.031	0.90	1.65	0.0048	0.013	0.7	0.051	0.002	0.98	0.11	−0.17	0.99
2	1.84	2.77	0.032	0.89	2.76	0.0049	0.037	0.83	0.103	0	0.98	0.23	−0.34	0.99
3	1.81	2.32	0.023	0.95	3.54	0.0020	0.025	0.7	0.103	0.107	0.98	0.23	−0.23	0.99

diffusion). Additionally, the negative values of I for surface diffusion indicates there are no boundary layer effects on the rate of adsorption.

4. Conclusion

The RSM model using the R software was chosen to evaluate the relationship between input independent factors (pH, SiO_2@Fe_3O_4@MBT dosage, time and initial As (V) concentration) and one dependent output response (removal efficiency) on As (V) sorption onto SiO_2@Fe_3O_4@MBT. The FSO model represented a satisfactory adjustment between the model and experimental data due to an insignificant lack of fit (p-value > 0.05), greater F-value, smaller p-value, and higher R^2 than the other models. The regression analysis of the FSO model showed that the terms of X_4: X_1: X_3, X_3: X_4 and X_1^2 with an oppositional effect and the terms of X_1, X_2, X_3, X_1: X_2, X_2: X_4 with a synergistic effect can be applied to the design of a predicted equation by the model, which can be used for prediction and optimization. The results indicated that SiO_2@Fe_3O_4@MBT with the maximum predicted removal percentage of 95.77% under the selected conditions (initial As (V) concentration, 1 mg L^{-1}; adsorbent dosage, 98.4 g L^{-1}; time, 178.4 min; pH, 6.55) has the required ability to adsorb As (V) from aqueous solutions. The experimental isotherm data best fit the Freundlich model than the other isotherms, indicating a multi-molecular layer adsorption, a heterogeneous system and the uneven adsorption of the adsorbate on the adsorbent surface. The maximum Langmuir adsorption capacity was 10.38, 11.35 and 17.5 mg g^{-1} for 291 K, 301 K and 311 K, respectively. Among the studied kinetics, the pseudo-first order kinetic model was found to give the best kinetic fitting.

Acknowledgement

This study is related to the project NO. 1396/66330 from Student Research Committee, Shahid Beheshti University of Medical Sciences, Tehran, Iran. We also appreciate the “Student Research Committee” and “Research & Technology Chancellor” in Shahid Beheshti University of Medical Sciences for their financial support of this study.

References

[1] M.A. Bezerra, R.E. Santelli, E.P. Oliveira, L.S. Villar, L.A. Escaleira, Response surface methodology (RSM) as a tool for optimization in analytical chemistry, Talanta 76 (5) (2008) 965–977.
[2] J. Han, et al., Effect of nitrogen doping on titanium carbonitride-derived adsorbents used for arsenic removal, J. Hazard. Mater. 302 (2016) 375–385.
[3] A. Najafpoor, Z. Vojoudi, M. Dehgani, F. Changani, H. Alidadi, Quality Assessment of the Kashaf River in North East of Iran in 1996–2005, 2007.
[4] M.M. Areco, S. Hanela, J. Duran, M. dos Santos Afonso, Biosorption of Cu (II), Zn (II), Cd (II) and Pb (II) by dead biomasses of green alga *Ulva lactuca* and the development of a sustainable matrix for adsorption implementation, J. Hazard. Mater. 213 (2012) 123–132.
[5] K. Sharafi, N. Fattahi, M. Pirsaheb, H. Yarmohamadi, M. Fazlzadeh Davil, Trace determination of lead in lipsticks and hair dyes using microwave-assisted dispersive liquid–liquid microextraction and graphite furnace atomic absorption spectrometry, Int. J. Cosmet. Sci. 37 (5) (2015) 489–495.
[6] Y. Li, G. Sheng, J. Sheng, Magnetite decorated graphene oxide for the highly efficient immobilization of Eu (III) from aqueous solution, J. Mol. Liq. 199 (2014) 474–480.
[7] Y.-S. Shen, S.-L. Wang, Y.-M. Tzou, Y.-Y. Yan, W.-H. Kuan, Removal of hexavalent Cr by coconut coir and derived chars–the effect of surface functionality, Bioresour. Technol. 104 (2012) 165–172.
[8] M. Xu, W. Linghu, J. Hu, G. Jiang, J. Sheng, Utilization of Mg 2 Al–layered double hydroxide as an effective sequestrator to trap Cu (II) ions from aqueous solution impacted by water quality parameters, J. Phys. Chem. Solids 98 (2016) 100–106.
[9] Q. Yuan, et al., Effect of large pore size of multifunctional mesoporous microsphere on removal of heavy metal ions, J. Hazard. Mater. 254 (2013) 157–165.
[10] M.A. Habila, et al., Mercaptobenzothiazole-functionalized magnetic carbon nanospheres of type Fe3, Microchim. Acta 183 (8) (2016) 2377–2384.
[11] R. Roto, Y. Yusran, A. Kuncaka, Magnetic adsorbent of Fe_3O_4@ SiO_2 core-shell nanoparticles modified with thiol group for chloroauric ion adsorption, Appl. Surf. Sci. 377 (2016) 30–36.
[12] S. Sultan, K. Kareem, L. He, Synthesis, characterization and resistant performance of α-F_e2O_3@ SiO_2 composite as pigment protective coatings, Surf. Coat. Technol. 300 (2016) 42–49.
[13] S. Zhang, et al., Thiol modified Fe_3O_4@ SiO_2 as a robust, high effective, and recycling magnetic sorbent for mercury removal, Chem. Eng. J. 226 (2013) 30–38.
[14] L. Lai, Q. Xie, L. Chi, W. Gu, D. Wu, Adsorption of phosphate from water by easily separable Fe_3O_4@ SiO_2 core/shell magnetic nanoparticles functionalized with hydrous lanthanum oxide, J. Colloid Interface Sci. 465 (2016) 76–82.
[15] B. Huang, et al., Effect of Cu (II) ions on the enhancement of tetracycline adsorption by Fe 3 O 4@ SiO 2-chitosan/graphene oxide nanocomposite, Carbohydr. Polym. 157 (2017) 576–585.
[16] F. Wang, et al., Fe_3O_4@ SiO_2@ CS-TETA functionalized graphene oxide for the adsorption of methylene blue (MB) and Cu (II), Appl. Surf. Sci. 420 (2017) 970–981.
[17] Q. Pu, Z. Su, Z. Hu, X. Chang, M. Yang, 2-Mercaptobenzothiazole-bonded silica gel as selective adsorbent for preconcentration of gold, platinum and palladium prior to their simultaneous inductively coupled plasma optical emission spectrometric determination, J. Anal. At. Spectrom. 13 (4) (1998) 249–253.
[18] M. Khajeh, Application of modified organo-nanoclay as the sorbent for zinc determination by FAAS: an optimization study of an online pre-concentration system, Biol. Trace Elem. Res. 145 (1) (2012) 118–125.
[19] M. Khayet, A. Zahrim, N. Hilal, Modelling and optimization of coagulation of highly concentrated industrial grade leather dye by response surface methodology, Chem. Eng. J. 167 (1) (2011) 77–83.
[20] J.-P. Wang, Y.-Z. Chen, Y. Wang, S.-J. Yuan, H.-Q. Yu, Optimization of the coagulation-flocculation process for pulp mill wastewater treatment using a combination of uniform design and response surface methodology, Water Res. 45 (17) (2011) 5633–5640.
[21] H. Alidadi, et al., Evaluation of clinoptilolite modified by cationic surfactant for nitrate removal from aqueous solutions, Journal of Research in Environmental Health 3 (1) (2017) 21–29.
[22] J.A. Wass, Design-Expert 5.0. Biotech Software & Internet Report, Comput. Softw. J. Scient 1 (3) (2000) 88–95.
[23] B. Jones, J. Sall, JMP statistical discovery software, Wiley Interdiscip. Rev. Comput. Stat. 3 (3) (2011) 188–194.
[24] Statgraphics Centurion, X, Statpoint Technologies Inc. Warrenton, USA, 2009.
[25] A. Sheikhmohammadi, et al., Application of graphene oxide modified with 8-hydroxyquinoline for the adsorption of Cr (VI) from wastewater: optimization, kinetic, thermodynamic and equilibrium studies, J. Mol. Liq. 233 (2017) 75–88.
[26] M. Pirsaheb, et al., Preparation of the activated carbon from India shrub wood and their application for methylene blue removal: modeling and optimization, Desalin. Water Treat. 57 (13) (2016) 5888–5902.
[27] A.-A. Salarian, et al., N-doped TiO 2 nanosheets for photocatalytic degradation and mineralization of diazinon under simulated solar irradiation: optimization and modeling using a response surface methodology, J. Mol. Liq. 220 (2016) 183–191.
[28] D.K. Yi, S.S. Lee, J.Y. Ying, Synthesis and applications of magnetic nanocomposite catalysts, Chem. Mater. 18 (10) (2006) 2459–2461.
[29] K. Sobolev, et al., Engineering of SiO2 nanoparticles for optimal performance in nano cement-based materials, Nanotechnology in Construction, Vol. 3, Springer 2009, pp. 139–148.
[30] D. Podstawczyk, A. Witek-Krowiak, A. Dawiec, A. Bhatnagar, Biosorption of copper (II) ions by flax meal: empirical modeling and process optimization by response surface methodology (RSM) and artificial neural network (ANN) simulation, Ecol. Eng. 83 (2015) 364–379.
[31] M. Gholami, et al., In vitro antibacterial activity of poly (amidoamine)-G7 dendrimer, BMC Infect. Dis. 17 (1) (2017) 395.
[32] H. Parham, B. Zargar, R. Shiralipour, Fast and efficient removal of mercury from water samples using magnetic iron oxide nanoparticles modified with 2-mercaptobenzothiazole, J. Hazard. Mater. 205 (2012) 94–100.
[33] R.H. Myers, D.C. Montgomery, C.M. Anderson-Cook, Response Surface Methodology: Process and Product Optimization Using Designed Experiments, John Wiley & Sons, 2016.
[34] H. Aslani, et al., Application of response surface methodology for modeling and optimization of trichloroacetic acid and turbidity removal using potassium ferrate (VI), Desalin. Water Treat. (2016) 1–12.
[35] R.V. Lenth, Response-surface methods in R, using rsm, J. Stat. Softw. 32 (7) (2009) 1–17.
[36] A.M. Bandpei, et al., Optimization of arsenite removal by adsorption onto organically modified montmorillonite clay: experimental & theoretical approaches, Korean J. Chem. Eng. 34 (2) (2017) 376–383.
[37] G.E. Box, K. Wilson, On the experimental attainment of optimum conditions, Breakthroughs in Statistics, Springer 1992, pp. 270–310.
[38] A.S. Mohammadi, M. Sardar, M. Almasian, Equilibrum and kinetic studies on the adsorption of penicillin g by chestnut shell, Environ. Eng. Manag. J. (EEMJ) 15 (1) (2016).
[39] M. Moradi, et al., The efficiency study of pumice powder to lead removal from the aquatic environment: isotherms and kinetics of the reaction, J. Mazandaran Univ. Med. Sci. 23 (1) (2014) 65–75.
[40] M. Moradi, L. Hemati, M. Pirsaheb, K. Sharafi, Removal of hexavalent chromium from aqueous solution by powdered scoria-equilibrium isotherms and kinetic studies, World Appl. Sci. J. 33 (3) (2015) 393–400.
[41] K. Naddafi, et al., Adsorption of 2, 4, 6-trichlorophenol from aqueous solutions by a surfactant-modified zeolitic tuff: batch and continuous studies, Desalin. Water Treat. 57 (13) (2016) 5789–5799.
[42] H. Godini, et al., Water polishing of phenol by walnut green hull as adsorbent: an insight of adsorption isotherm and kinetic, J. Water Reuse Desalin. 6 (4) (2016) 544–552.
[43] D. Ociński, I. Jacukowicz-Sobala, P. Mazur, J. Raczyk, E. Kociołek-Balawejder, Water treatment residuals containing iron and manganese oxides for arsenic removal

from water–characterization of physicochemical properties and adsorption studies, Chem. Eng. J. 294 (2016) 210–221.
[44] Y. Sun, et al., Direct synthesis of bacteria-derived carbonaceous nanofibers as a highly efficient material for radionuclides elimination, ACS Sustain. Chem. Eng. 4 (9) (2016) 4608–4616.
[45] X. Wang, et al., High sorption of U (VI) on graphene oxides studied by batch experimental and theoretical calculations, Chem. Eng. J. 287 (2016) 448–455.
[46] R. Ocampo-Pérez, J. Rivera-Utrilla, J.D. Méndez-Díaz, M. Sánchez-Polo, Modeling adsorption rate of organic micropollutants present in landfill leachates onto granular activated carbon, J. Colloid Interface Sci. 385 (1) (2012) 174–182.
[47] S.I. Rathnayake, Y. Xi, R.L. Frost, G.A. Ayoko, Environmental applications of inorganic–organic clays for recalcitrant organic pollutants removal: bisphenol A, J. Colloid Interface Sci. 470 (2016) 183–195.
[48] M. Massoudinejad, M. Ghaderpoori, A. Shahsavani, M.M. Amini, Adsorption of fluoride over a metal organic framework Uio-66 functionalized with amine groups and optimization with response surface methodology, J. Mol. Liq. 221 (2016) 279–286.
[49] H. Liu, et al., Removal of cephalexin from aqueous solutions by original and Cu (II)/Fe (III) impregnated activated carbons developed from lotus stalks kinetics and equilibrium studies, J. Hazard. Mater. 185 (2) (2011) 1528–1535.
[50] Y. Ma, Y.-M. Zheng, J.P. Chen, A zirconium based nanoparticle for significantly enhanced adsorption of arsenate: synthesis, characterization and performance, J. Colloid Interface Sci. 354 (2) (2011) 785–792.
[51] Z. Veličković, et al., Adsorption of arsenate on iron (III) oxide coated ethylenediamine functionalized multiwall carbon nanotubes, Chem. Eng. J. 181 (2012) 174–181.
[52] M.N. Sepehr, et al., Defluoridation of water via light weight expanded clay aggregate (LECA): adsorbent characterization, competing ions, chemical regeneration, equilibrium and kinetic modeling, J. Taiwan Inst. Chem. Eng. 45 (4) (2014) 1821–1834.